Experimental and Numerical Investigation of Flow Field Structure over Swept Back Wing

[1]Samrat Biswas, [2]Animesh Roy, [3]Prabir Kr. De, [3]Bireswar Majumdar
[1]PhD Research Fellow, [2]PhD Research Fellow, [3]Professor, [4]Professor
[1, 2, 4]Department of Power Engineering, Jadavpur University, Kolkata, India
[3]Department of Mechanical Engineering, Jadavpur University, Kolkata, India

Abstract : To investigate swept-back wing configuration designed using supercritical RAE 2822 airfoil, experimental and numerical methods have been implemented. The study conducted with the wing model of aspect ratio 4, taper ratio 0.6 and was tested at Mach number 0.04 between pitch angle range of 0° and 30° in the open type subsonic wing tunnel. Numerical studies have also been performed using one equation model of Spalart-Allmaras on this wing under similar conditions. Experimental lift coefficient (C_L) is calculated from data obtained using force measuring balance. Numerical results were analyzed along-side experimental data and presence of pseudo-stall was observed at around 10° AoA. Static pressure distribution measurements over wing leeward surface were acquired over six chord-wise measuring section distributed along half span of wing. And these data were also compared with numerically obtained surface pressure distribution data. The results indicated formation and development of laminar separation bubble over wing leeward surface. Several different flow regimes -laminar separation, separation bubble, bubble extension, and 3D flow were observed and analyzed. In addition to complement surface pressure distribution results and to further analyze the flow field structure around the wing model numerically calculated pathline data were also discussed. Pathline results further clarified the observation found during surface pressure distribution analysis.

IndexTerms - Supercritical wing; pseudo-stall phenomena; lift coefficient; surface pressure coefficient distribution; pathline.

Nomenclature:

$AR = b^2 / S$	Aspect ratio
b	Span
C_L	Coefficient of lift
C_p	Coefficient of pressure
C_r	Wing root chord
C_t	Wing tip chord
Exp	Experimental Value
M	Mach number
MAC	Mean aerodynamic chord
Num	Numerical Value
Re_{MAC}	Reynolds number using MAC
$s = (b / 2)$	Half span
α	Angle of attack (AoA)
$\Lambda_{c/4}$	Swept angle

I. INTRODUCTION

Aircraft wing design starts with selection of airfoil section from myriad of choices. It is desirable that these airfoils have low drag and stability at cruising speed (Abbott & Von Doenhoff, 1959). One of most classical problem in aerodynamics is calculation of pressure coefficient distribution over different airfoil configuration. Post World War II massive improvement in propulsion technology and aerodynamics lead to requirement of high speed and fuel efficient operation of aircraft. For military application as well as commercial application swept wing application became prevalent.

In 1970s Whitcomb developed concept of supercritical airfoil (Wallace, Lane, & Mack, 1998). These supercritical airfoils can operate at higher critical Mach no. without producing wave drag. Implementation of swept back wing design along with supercritical airfoil has greatly improved the characteristics of wing behavior in transonic region. NASA during testing of modified F-8 crusader at Dryden flight research center first implemented supercritical wing design.

During late 1950s lot of experimental works has been carried out on swept-back wings in NASA (previously known as NACA). Some of these literatures were declassified recently; among those literatures it has been found that Haines and Rhodes (Haines & Rhodes, Tests in The R.A.E. 10ft x 7ft High Speed Tunnel on Three Wings With 50 deg Sweepback and 7-5 Percent Thick Sections, 1954) conducted experiments in royal aircraft establishment having 10ft x 7ft high speed wind tunnel in 1954. They conducted experiments on 3 types of swept back wings. Two of them had aerofoil section RAE 101 (maximum thickness 0.31c) and aspect ratio of 3.1 and 3.5 respectively. Third one was thicker further aft (towards tail) 0.4c, aspect ratio 3.1 and having

effectively sharper nose than RAE 101. Swept angle of all three wings was kept 30°. Experiments were conducted at Reynolds number 2 x 10^6 and in between Mach no. 0.50 and 0.95. results concluded that at some incidence, the laminar boundary layer separates from close to the leading edge near the inbound end of the curved tip. Further increase in incidence, the area affected by this separation extends inward and rearward. A part span vortex sheet originates from near the leading edge at the inboard end of this region of separation and trails back across the wing. Projection of flow sheet on wing surface bent outward to the free stream direction. Haines (Haines, Some Notes On The Flow Patterns Observed Over Various Swept-Back Wings At Low Mach Numbers (in The 10ft x 7ft High Speeed Tunnel), 1954) further experimented over ten swept back wings at high incidence and low Mach number using same wind tunnel. In all those experiments it was observed that wings suffer from a leading edge separation. Relations between regions of flow separation, together with associated part-span vortex sheets with different angle of incidence and Reynolds number and wing design were also discussed.

In 1970s after formation of North Atlantic Treaty Organization's Advisory Group for Aerospace Research and Development (AGARD), series of experiments were carried out by aerodynamicists and later those experimental results were used to validate numerical codes. Among those experiments Cook et. al. (Cook, Mcdonald, & Firmin, 1979) studied the 2D configuration of RAE 2822 in 8-ft x 6ft transonic wind tunnel at Mach numbers ranging from 0.676 to 0.740 and chord based Reynolds number varied from $5.7x10^6$ to $2.7x10^6$. Angle of incidence was kept between 2.40° and 3.19°. Data included surface pressure measurements and mean flow boundary later and wake profiles deduced from traverse of pitot and static pressure measuring probes.

Treadgold et. al. (Treadgold, Jones, & Wilson, 1979) conducted experiment on RAE wing 'A' (RAE 101 section) in combination with an axi - symmetric body within transonic region at Mach numbers 0.4, 0.8 and 0.9 in a Royal Aircraft Establishment 8ft x 6ft transonic wind tunnel. The pressure distribution over the wing-body combination was measured and also studied.

In 1990s development in efficient and affordable computation power brought forward numerical technique as choice for method of analysis. Slater (Slater J. W., 1998) in 1998 demonstrated the computation results of flow over RAE 2822 airfoil section for two-dimensional turbulent, transonic flows about an airfoil. The study was validated using experimental results obtained from Cook et. al. (Cook, Mcdonald, & Firmin, 1979). In 2000 Slater (Slater J. W., NPARC Alliance CFD Verification and Validation, 2000) did numerical study to verify the experimental results from the previously mentioned paper of Cook et. al. (Cook, Mcdonald, & Firmin, 1979) at low Mach number 0.3 and zero angle-of-attack. Later in 2002 Slater (Slater J. W., NPARC Alliance CFD Verification and Validation, 2002) did numerical study of RAE 2822 transonic airfoil and validated results against the experimental data obtained from Cook et. al. (Cook, Mcdonald, & Firmin, 1979). During the numerical study Spalart-Allmaras turbulence model (Spalart & Allmaras, 1994) was used to validate the results.

Most of these experimental investigations are confidential in nature because of commercial and defense purposes. Despite the obvious desirability of achieving a fundamental understanding of these low-speed phenomena problems occur during landing, take-off, mid-air maneuvering etc., most of the solutions for military aircrafts were reached in an empirical manner through wind-tunnel studies guided by only qualitative understanding of the phenomena involved. It was also observed in available literatures that most of these experiments were conducted in high-subsonic or transonic regions.

In recent times advancements in technology, helped to develop small scaled aircrafts like Unmanned Ariel Vehicle (UAVs) or Remote Piloted Vehicles (RPVs). These small scale aircrafts were designed to be used for commercial, defense and scientific exploration purposes. These MAVs are often required to operate within large range of Reynolds number, which is significantly below half a million. Also normal sized aircrafts during landing, take-off and mid-air maneuvering conditions operate in low subsonic range. Hence it further raises question regarding the requirement of knowledge regarding behavior of airfoils and wings in low Reynolds number region.

Now-a-days most of the aircrafts implement swept back wing design along with supercritical airfoil to achieve high fuel efficiency during high cruising speed operation. It is considered for the present investigation to analyze the structure of flow field around the swept-back tapered wing configuration during take-off, landing and maneuvering or operation specifically during low Reynolds number operation.

II. EXPERIMENTAL FACILITY

For the present investigation wind tunnel located at Fluid Mechanics and M/C Laboratory, Dept. of Power Engineering, Jadavpur University, Kolkata, India is used to perform experiments. The wind tunnel is open-loop, suction-type, and low-turbulence wind tunnel having 0.6 m×0.6 m test section. Figure 1 shows schematic diagram of wind-tunnel. The free-stream velocity (u_∞) was measured with help of Pitot - static tube. Multiple turbulence screens and aluminum honeycomb structure installed upstream at a 9:1 contraction section, helping to produce free-stream turbulence intensity of less than 0.1%. Average velocity non-uniformity across the cross section was less than 0.5%.

Wing model of 30° tapered, swept back designed using RAE 2822 airfoil is considered for the investigation. Geometry of airfoil is shown in the Figure 2 made available from UIUC applied aerodynamics group (Selig, 2018). Details regarding geometry of the wing model are given in Table 1. Plan form view of wing model is given in Figure 3. The entire set of experiment is carried out at a free- stream velocity (u_∞) of 12m/s at Reynolds number of 5.95×10^4 based on mean aerodynamic length. A two axis model positioning system with motorized movement of α pitch angle, ranging from -10° to +30° is used to orient wing model in test section. Data was recorded in between of 0° and 30° angle of attack. Lift coefficient were calculated using balance recorded raw data with the help of in-house written numerical code.

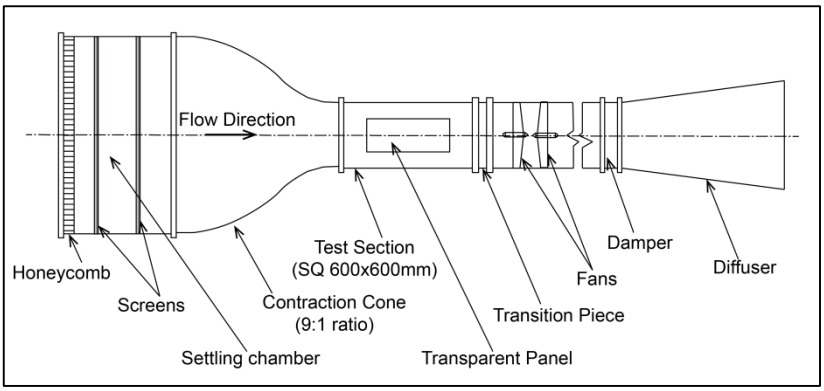

Figure 1 Schematics diagram of wind tunnel

Table 1. Geometric Parameters of Wing

area of the wing model S, m^2	233.4784x10^{-4}
aspect ratio $AR = b^2 / S$	4
span b, m,	0.3056
swept angle $\Lambda_{c/4}$, deg	30°
taper ratio λ	0.6
wing root chord C_r,m	0.0955
wing tip chord C_t,m	0.0573

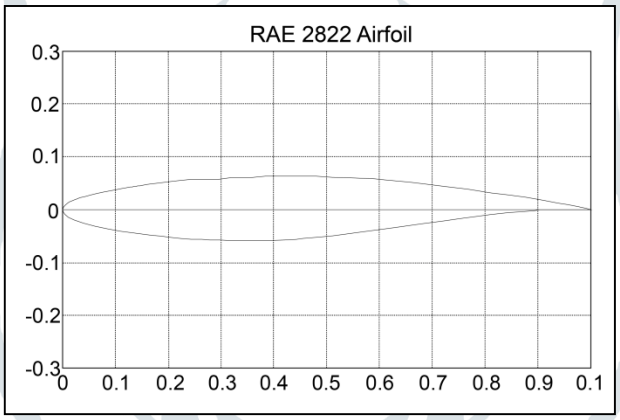

Figure 2 Geometry of RAE2822 airfoil

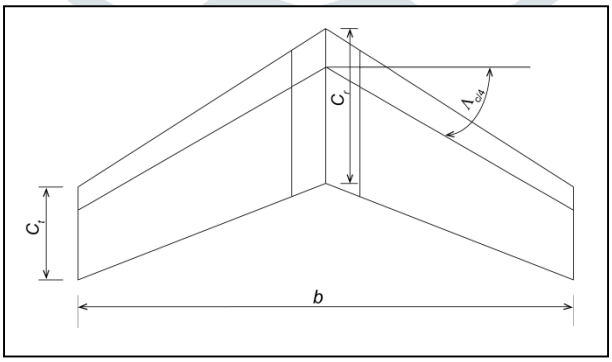

Figure 3 Geometry of wing model

The locations of pressure taps were located on half portion of wing model considering the symmetry condition is shown in Figure 4. The positions of pressure taps were not only issue of importance but manufacturing of those taps were also a matter of engineering challenge. It has also been considered that pressure taps should cover whole half span of the wing model because of symmetry exist between both half span of wing model. It has also been taken into consideration for position of pressure taps that the effect caused by one of the pressure taps should make little or no interfere with flow over other pressure taps. Wing span was separated in six numbers of pressure measurement sections at y / s = 0.26 (a-section), 0.39 (b-section), 0.52 (c-section), 0.62 (d-section), 0.79 (e-section), and 0.92 (f-section) were placed on the wing surface, where s *(b / 2)* indicating half span. Two of the six sections are placed near inboard portions and another two stations were placed near outboard portions of wing. And remaining two sections were placed in middle portion of wing. Four pressure tap stations were distributed on each station along the chord-wise direction. Twenty four designed pressure taps were distributed over the leeward surface of wing.

Pressure taps distributed over wing surface were connected to pressure transmitter inlet using PVC tubes. Those PVC tube were routed through hollow internal portion of wing model. Furthermore pressure sensed at each pressure taps data were measured using electronic pressure transmitter made by Kimo, France. It has Configurable Range in between -10,000Pa to +10,000Pa. And according to specification minimum configurable range lies within 0Pa to ±1000Pa. It has interchangeable measuring range and permanent self calibration. The pressure transmitter has two ports to facilitate insertion of tubes through which differential pressure can be measured. The transducer present inside the transmitter measures the difference in pressure between two tubes. This measurement is performed by measuring the strain in a thin element using an electronic strain gauge. The strain gauge converts these value into corresponding voltage hence the pressure is measured. Pressure readings are displayed on a LCD Display attached on the device, from which the data were noted.

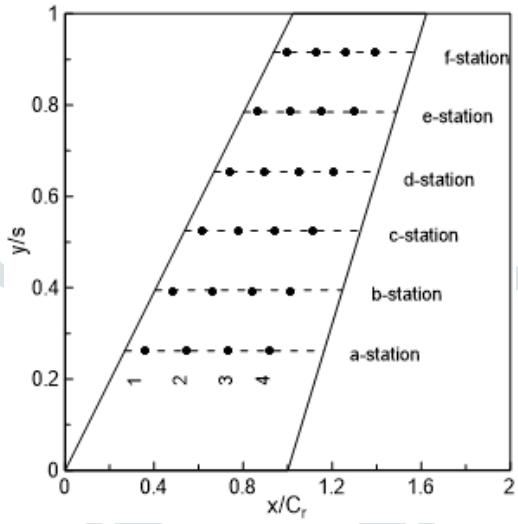

Figure 4 Location of pressure orifices

III. NUMERICAL FACILITY

The wing model is also numerically simulated using Spalart-Allmaras (SA) turbulence model. Spalart-Allmaras model was developed mainly for external flow over airfoil and wings (aerospace applications).

Geometry of the swept-back wing is created in CAD software. Un-structured hybrid mesh grids are generated using Ansys ICEM CFD, which are combinations of tetrahedron, wedge and pyramids meshing. Results obtained from different sized mesh sizes having different number of cells e.g., 156655, 183395, 320636, 694714 etc. for Reynolds number of 5.95×10^4 based on mean aerodynamic chord at α =10° were compared with experimental data to ensure grid independence. It was decided to conduct further simulations using 320636 numbers of cells. Since the difference between results of C_L value obtained from numerical calculation and experimental measurement were found to be negligible with further refinement of mesh sizes, which is given in Table 2.

Figure 5 shows sectional view of full mesh. Near wall mesh sizes (average y^+ values of 1.5) are arranged appropriately to resolve the boundary velocity profile. Total 79008 numbers of nodes and 320636 numbers of elements are created in mesh. The mesh statistics are given in Table 3 and according to mesh quality criteria of ANSYS mesh quality improves significantly as value of orthogonal quality of mesh moves towards 1. Average mesh orthogonal quality found to be 0.83 for the present investigation. The mesh average skewness of the generated mesh has been maintained at 0.28.

Table 2 Results of different mesh configuration

AoA = 10°	Number of cell	C_L
Experimental Data	-	0.66
Mesh Config. 0	156655	0.69
Mesh Config. 1	183395	0.69
Mesh Config. 2	320636	0.65
Mesh Config. 3	694714	0.65

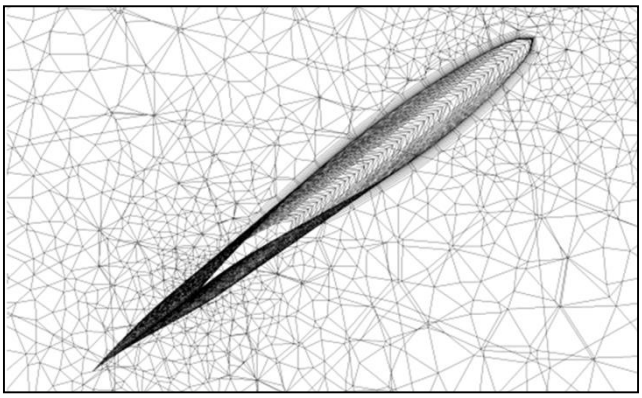

Figure 5 Cross-sectional view of the grid structure over wing

Table 3 Mesh Statistics

mesh metric	minimum	maximum	average
orthogonal quality	$2.45x10^{-002}$	0.99	0.83
skewness	$1.12x10^{-003}$	0.98	0.28

Table 4 Parameters for Numerical Calculation

gas	air, ideal gas
density	1.177 kg/m3
viscosity	1.853e-05 kg/m-s
M	0.04
velocity	12 m/s
temperature	300 k

Density and viscosity are assumed for the prevailing flow without any significant change in temperature which in given in Table 4. Pressure-velocity coupling method with second order upwind spatial discretization scheme is used. Solution was initialized uniformly throughout the domain using free stream inlet condition. Velocity inlet with free stream velocity magnitude of 12 m/s is used as inlet boundary condition. No-slip wall condition is applied to the model surfaces. To simulate angle of attack stream velocity directions are adjusted in accordance to required angle of attack. A convergence criteria of 10^{-3} is selected for the residuals. Various details like pressure, velocity, surface streamlines etc were obtained for comparison with experimental results.

IV. Results and Discussion

Figure 6 shows profile plots of the lift coefficient (C_L) obtained both numerically and experimentally by changing AoA for wing model.

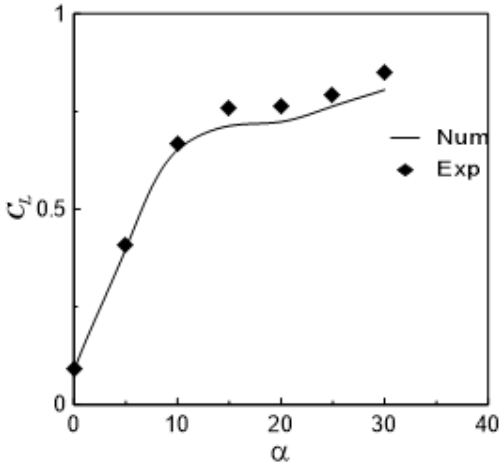

Figure6 Lift coefficient (C_L) over wing model.

In Figure 6 x-axis represents change in angle of attack (α) and y-axis shows lift coefficient (C_L). It can be seen from the figure the lift coefficient C_L increases with α up to about 9° angle of attack. But the lift coefficient starts to drop near 15° α. Lift typically starts to fall when boundary layer transited from attached flow to separated flow.

This lift-fall phenomenon may be termed as "pseudo-stall". Numerical results also predict presence of "pseudo-stall" behavior along with experimental data characteristics at around the same location. it is observed that slope of C_L curve starts to increase again at about 20° AoA may because of the onset of turbulent flow over the wing. The lift rise phenomenon is induced from the reaction of the scavenging effect on the suction surface as observed by Hoerner and Borst (Hoerner & Borst, 1975). From this curve it can be deduced logically that lift characteristics of the wing may be strongly affected by complex behavior of the boundary layer flow over the surface and also due to 3D flow structures originating from the end effects.

4.1 Surface Cp distribution

Figure 7 illustrates the chord wise pressure coefficient (C_p) distribution of different measuring sections for wing model at several different angle of attacks for both experimental and numerically calculated data. Here the pressure coefficient (C_p) is plotted against x / c. Where x is distance along wing in chord-wise direction and c is the length of local chord of wing model at measuring sections. In this figure row wise plots starting from the extreme top end to bottom represent six different measuring section a, b, c, d, e and f-section respectively. Where a and b-section lies in inboard section, c and d-section lies near middle portion and e and f section lies at outboard portion of wing. And column-wise initiating from left to the right plots represent four different angle of attacks 0°, 10°, 15° and 20° respectively under investigation. Plot were compiled and represented in such a way to facilitate comparative study and to observe change in pressure coefficient distribution along chord-wise direction on leeward surface of wing with change in measuring section and angle of attack.

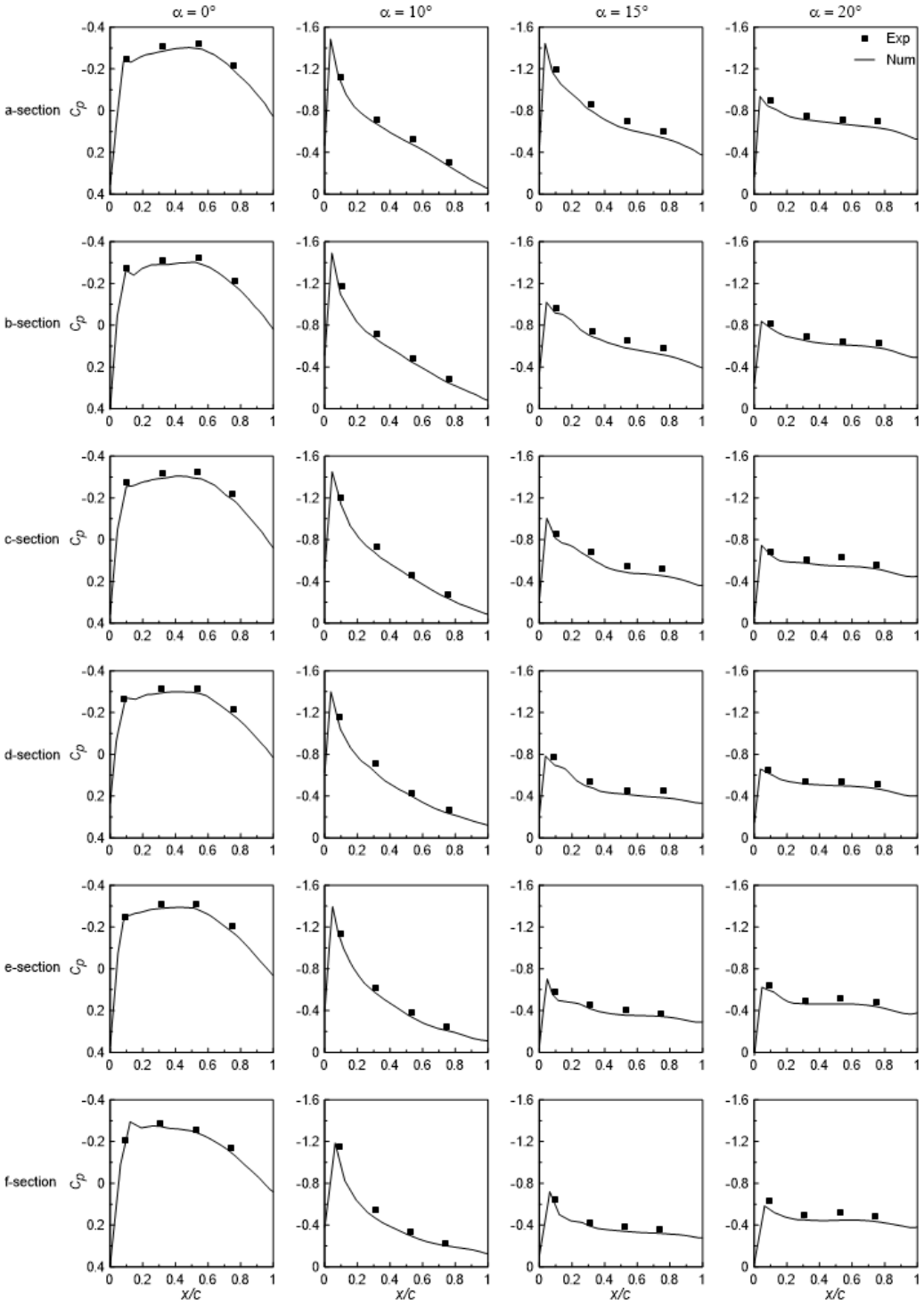

Figure 7 Plot of surface pressure distribution over wing leeward surface measuring station

The airfoil section used for the wing modeling has a finite thickness distribution, which leads to favorable pressure gradient over a large part of the airfoil under low angle of attacks (Bertin & Smith, 1989). In Figure 7 left most columns represent the pressure coefficient distribution at 0° angle of attack. It can be observed that at 0° AoA over significant portion of wing leeward surface favorable pressure gradient persists along the chord-wise direction. For all the measuring section starting from a to f section significant portion of airfoil showed favorable pressure gradient along chord wise direction. Since a-section and b-section lies near the inboard section of the wing it has greater portion of airfoil favorable pressure gradient compared to outboard section containing e-section and f-section. Furthermore, this represents that the flow over significant part of wing model remains attached to surface along chord-wise direction. It is already known from the literature that region of the wing surface having favorable pressure gradient have $dC_p / dx < 0$. And increment of value of C_p negatively, indicate creation of more strong suction force over wing leeward surface. Inversely wing surface having $dC_p / dx > 0$, is known as adverse pressure gradient, where the value of C_p increases positively but the magnitude of C_p decreases, or C_p become less negative.

At 10° angle of attack it can be observed that as we move toward downstream location from suction peak in C_p near tip of airfoil, the rate of pressure coefficient slope decrease along chord-wise direction. It can be further deduced that at 10° AoA laminar

separation occurs over wing surface. With increase in angle of attack it can also be observed that compared to 0° angle of attack at 10° pressure coefficient increases more negatively near wing tip. Near inboard measuring section at a-section and b-section decrease in slope of pressure gradient observed to be steeper compared to mid-section at c-section and d-section. There is no indication of plateau in pressure gradient curve points towards absence of laminar separation bubble over the wing surface. Near outboard section in e-section, f-section C_p value near tip of wing reaches less negative value than inboard and mid-section of wing.

From Figure 7 it can be seen that as the angle of attack increases to 15° angle of attack the possible formation of laminar separation bubble takes place. No indication of local separation or sectional stall in inboard a-section pressure distribution at 15° AoA. Formation of laminar separation bubble over wing manifests itself as fairly constant pressure in the region of bubble formation and points towards the presence of local separation of flow (Gaster, March 1967). Staring from b-section onwards up to f-section pressure plateau close to leading edge of the wing can be observed for 15° angle of attack. For b-section this pressure plateau covers the region of approximately within $0.04 \leq x/c \leq 0.20$. Middle portion of wing in c-section and d-section it can be seen that the pressure plateau remain within close proximity of each other, which is in the range of $0.10 \leq x/c \leq 0.22$ and $0.10 \leq x/c \leq 0.21$ respectively. Near outboard section of wing e-section and f-section the region of laminar separation bubble appears to be lies within $0.11 \leq x/c \leq 0.26$ and $0.12 \leq x/c \leq 0.26$ respectively.

And right most column of the Figure 7 represents the 20° angle of attack. And here it can be observed that with further increase in angle of attack from 15° to 20° the magnitude of pressure coefficient attains less negative value near the wing tip, creating less suction over the wing surface. Also it can be seen that with increase in angle of attack, the length of the region of constant pressure increases in size all the section throughout wing. Wing inboard portion near root in the a-section and b-section the pressure plateau lies approximately within $0.22 \leq x/c \leq 0.71$ and $0.20 \leq x/c \leq 0.84$ respectively. And for middle section of wing in c and d-section it can be seen that constant pressure region get increased compared to 15° AoA and remain within range of $0.18 \leq x/c \leq 0.78$ and $0.17 \leq x/c \leq 0.82$ respectively. And near outboard measuring sections of the wing increase in region of pressure plateau compared to 15° AoA can also be seen in Figure 7. In e-section and f-section the region of pressure coefficient plateau remains approximately within $0.16 \leq x/c \leq 0.70$ and $0.12 \leq x/c \leq 0.68$ respectively.

4.1 Pathline

Pathlines are trajectories that individual fluid particles follow. Or these can be thought of as "recording" the path of a fluid element in the flow over a certain period. From previous observation it can be deduced that numerically calculated values closely follows experimentally calculated ones. All the pathlines in present investigation are created from the numerical calculations to better understand the flow physics around the wing.

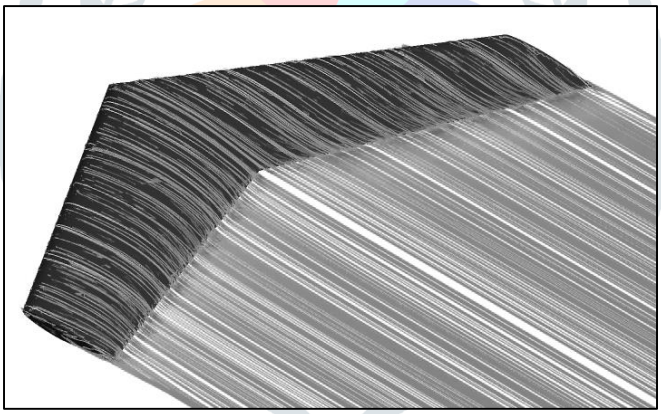

Figure 8(a) Pathline at 0° angle of attack

In Figure 8(a) computed pathlines are plotted at angle of attack 0°. It can be clearly seen from Figure 8(a) that there is no vortices present in the flow. Flow remains attached to the body and are laid out as a fine straight line in the flow field, which creates a negative pressure on the upper surface and helps to generate lift.

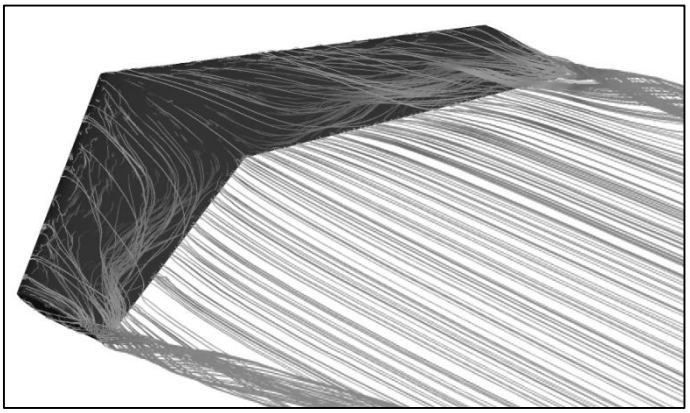

Figure 8(b) Pathline at 10° angle of attack

In Figure 8(b) represents the pathlines for angle of attack 10°. Here it can be observed that vortices stars to appear near the wingtip region. The rest of the flow remains attached. Here positive pressure region appears near the trailing edge region. Some of the flow from the wing leading edge gets pushed towards the wing tip to feed vortices near wing tip. And near inboard section and middle section of wing pathlines seems to be effected by heavy span-wise flow.

In Figure 8(c) depicts pathlines created for wing operation at 15° angle of attack. Presence of heavy span-wise flow can still be observed over wing surface. From Figure 8(c) it can be seen that portion of flow coming from wing leading edge portion gets deflected above leeward surface of wing creating vortical structure. In middle section this phenomena gets more pronounced and this flow comes back down and because of presence of heavy span-wise flow this flow gets pushed towards outboard section of wing. Near the wing tip region we observe that leakage of flow for finiteness of wing help to create swirling structure or wing tip vortex.

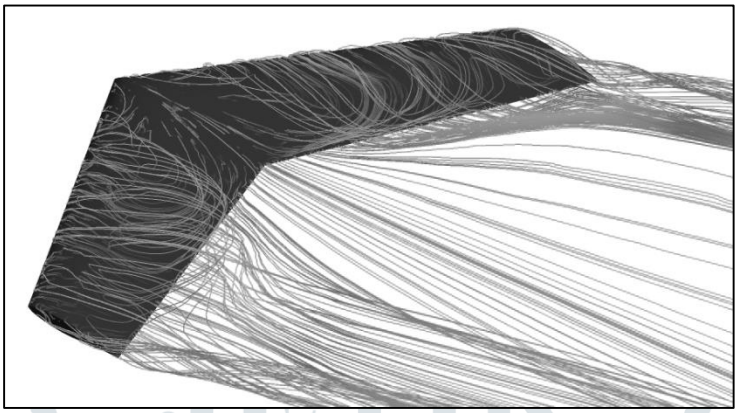

Figure 8(c) Pathline at 15° angle of attack

At 20° angle of attack which is shown in the Figure 8(d). It is observed that the size of the swirling structure over wing surface originating from wing leading edge flow gets increased. Here the swirling structures create a three dimensional flow because of the presence of span-wise direction flow influence. It can be seen that these three dimensional flow vortical structures originate from leading edge of wing and get merged with the vortices of the wingtip under the effect of heavy span-wise flow. Lift from wing is generated by the attached airflow over it from front to rear. With increasing span -wise flow boundary layer on surface of the wing have longer path to travel, and so are thicker and more susceptible to transition into turbulence or flow separation. So from the flow pattern at angle of attack 20° it can be deduced that the generation of lift get diminished because of the presence of flow separation.

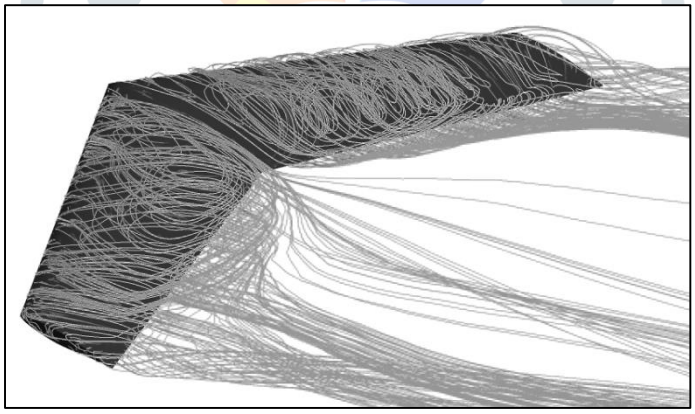

Figure 8(d) Pathline at 20° angle of attack

V. CONCLUSION

From the present investigation the following conclusions can be drawn about tapered swept back wing model made using of RAE2822 supercritical airfoil profile operating under highly subsonic range.

The surface pressure distribution of wing model at α=0°, 10°, 15°, 20° were investigated both experimentally and numerically simulated under similar conditions. Characteristics pathline flow patterns were also studied using numerically obtained results.

From experimental as well as numerical C_L, curve, it can be observed that lift increases up until "pseudo-stall" then the lift start to decrease. After the "pseudo-stall" phenomena lift starts to increase again.

Surface pressure distribution over leeward surface results showed formation of localized region of separation bubble or region of constant pressure coefficient plateau at 15° angle of attack. It was also found at 15° angle of attack this region of pressure plateau is greater in outboard and middle section compared to inboard section. And it was also found that with increase in angle of attack to 20° the region of pressure plateau seems to get increased along chord-wise direction.

Further to investigate flow field structure over wing model numerically computed pathline were analyzed. It showed that at low 0° angle of attack, flow remains mostly attached to the body and generates lift. As angle of attack increases to 10° effect of span-wise flow along the wing gets pronounced. And also manifestation of wing tip vortices structure because of flow leakage near wing tip can also be found. Finiteness of wing model causes flow slippage at wing tip.

At 15° angle of attack size of the vortices starts to increase resulted in localized formation of separation bubble. With increase in angle of attack from 15° to 20° it was found that size of localized separation bubble get increase in line with previous discussion made during surface pressure coefficient curve analysis. It intended to more in depth study of the flow features over supercritical wing in subsonic region at different orientation.

Numerical data showed overall good agreement with the experiment in context of lift coefficient, surface pressure coefficient distribution along chord-wise direction are well justified by Spalart-Allmaras turbulence model. Computed results are found to vary on average within 12% of the experimentally obtained results.

REFERENCES

[1] Abbott, I. H., & Von Doenhoff, A. E. (1959). Theory of Wing Sections, including a summery of airfoil data. Courier Corporation.

[2] Wallace, Lane, E., & Mack, P. E. (1998). The Whitcomb Area Rule: NACA Aerodynamics Research and Innovation. From Engineering Science to Big Science. (P. E. Mack, Ed.) Washington, D.C.: University Press of the Pacific.

[3] Haines, A. B., & Rhodes, C. W. (1954). Tests in The R.A.E. 10ft x 7ft High Speed Tunnel on Three Wings With 50 deg Sweepback and 7-5 Percent Thick Sections. NACA.

[4] Haines, A. B. (1954). Some Notes On The Flow Patterns Observed Over Various Swept-Back Wings At Low Mach Numbers (in The 10ft x 7ft High Speeed Tunnel). NACA.

[5] Cook, P. H., Mcdonald, M. A., & Firmin, M. C. (1979). Airfoil RAE 2822 - Pressure Distributions, and Boundary Layer and Wake Measurements, "Experimental Database FOr COmputer Program Assessment. NACA.

[6] Treadgold, D. A., Jones, A. F., & Wilson, K. H. (1979). Pressure Distribution In The RAE 8ft x 6ft Transonic Wind Tunnel On The RAE Wing 'A' In Combination With An Axi-Symmetric Body At Mach Numbers 0.4, 0.8, and 0.9. AGARD AR. 138, .

[7] Slater, J. W. (1998, September 30). NPARC Alliance Validation Archive. (NASA, Producer) Retrieved from NPARC Alliance CFD Verification and Validation: https://www.grc.nasa.gov/www/wind/valid/raetaf/raetaf01/raetaf01.html

[8] Slater, J. W. (2000, January 7). NPARC Alliance CFD Verification and Validation. Retrieved from NPARC Alliance Validation Archive: https://www.grc.nasa.gov/www/wind/valid/raetaf/raetaf02/raetaf02.html

[9] Slater, J. W. (2002, May 3). NPARC Alliance CFD Verification and Validation. (NASA) Retrieved from NPARC Alliance Validation Archive: https://www.grc.nasa.gov/www/wind/valid/raetaf/raetaf04/raetaf04.html

[10] Spalart, P. R., & Allmaras, S. R. (1994). A One Equation Turbulence Model for Aerodynamic Flows. La Recherche Aerpspatiale , 1, 5-24.

[11] Selig, M. (2018). Retrieved 2018, from UIUC Applied Aerodynamics Group, Department of Aerospace Engineering, University of Illinois : http://m-selig.ae.illinois.edu/ads/coord_database.html

[12] Hoerner, S. F., & Borst, H. V. (1975). Fluid-Dynamic Lift (second ed.). (H. V. Borst, Ed.) Brick Town, NJ, USA: Mrs. Liselotte A. Hoerner.

[13] Bertin, J. J., & Smith, M. L. (1989). Aerodynamics for Engineers (2nd Edition ed.). NJ: Prentice-Hall.

[14] Gaster, M. (1967 March) "The Structure and Behaviour of Laminar Separation Bubbles," Reports and Memoranda No. 3595 NPL Aero Report 1181, A.R.C. 28.226.